Warmer western tropical South Atlantic during the Last Interglacial relative to the current interglacial period

R.A. Nascimento, M.H. Shimizu, I.M. Venancio, C.M. Chiessi, H. Kuhnert, H.J.H. Johnstone, A. Govin, D. Lessa, J.M. Ballalai, P. Piacsek, et al.

Global and Planetary Change 215 (2022) 103889

Contents lists available at ScienceDirect

Global and Planetary Change

journal homepage: www.elsevier.com/locate/gloplacha

Warmer western tropical South Atlantic during the Last Interglacial relative to the current interglacial period

R.A. Nascimento [a,*], M.H. Shimizu [b], I.M. Venancio [a,d], C.M. Chiessi [c], H. Kuhnert [d], H.J.H. Johnstone [d], A. Govin [e], D. Lessa [a], J.M. Ballalai [a], T.P. Santos [a], P. Piacsek [f], S. Mulitza [d], A.L.S. Albuquerque [a]

[a] Programa de Geociências (Geoquímica), Universidade Federal Fluminense, Niterói, Brazil
[b] General Coordination of Earth Science, National Institute for Space Research, São José dos Campos, Brazil
[c] School of Arts, Sciences and Humanities, University of São Paulo, São Paulo, Brazil
[d] MARUM - Center for Marine Environmental Sciences, University of Bremen, Bremen, Germany
[e] Laboratoire des Sciences du Climat et de l'Environnement/Institut Pierre Simon Laplace, CEA-CNRS-UVSQ, Université Paris Saclay, Gif sur Yvette, France
[f] Centro de Geociencias, Universidad Nacional Autónoma de México, Juriquilla Querétaro, Mexico

ARTICLE INFO

Editor: Dr. Fabienne Marret-Davies

Keywords:
Last Interglacial
Western tropical South Atlantic
Mg/Ca-based Sea surface temperature

ABSTRACT

The Last Interglacial (LIG, 129–116 thousand years ago) is an excellent case study for global warming scenarios and a target for proxy-model comparisons. The LIG global average sea surface temperature (SST) was ~0.5 °C higher than pre-industrial (PI). Contrary to the global average, tropical SST proxy compilations and model simulations show a negative anomaly in LIG SST relative to PI. Here, we present a LIG SST record from marine sediment core GL-1180 retrieved from the western tropical South Atlantic (WTSA). The SST record is based on Mg/Ca ratios of planktonic foraminifera *Globigerinoides ruber* (white). Our results indicate a warmer LIG in the WTSA relative to PI and Holocene conditions. We show that a positive LIG SST anomaly in tropical regions can be explained by polar sea ice loss during the LIG, which warms the ocean surface all the way into the tropics. The disagreement between proxy results and model simulations from the fourth phase of the Paleoclimate Modelling Intercomparison Project could result from uncertainties in our proxy for SST and/or limitations of numeric models in capturing transient forcings and feedbacks in Earth's climate system and imprecise boundary conditions. Additional studies are warranted to better constrain the LIG SST evolution in tropical regions.

1. Introduction

The Last Interglacial (LIG), a warm period between 129 and 116 thousand years ago (ka), can be used as a case study for understanding the impact of global warming on continental ice volume and sea level change, as well as a validation target for climate models (Otto-Bliesner et al., 2017; Kageyama et al., 2018; Capron et al., 2014). During the LIG the sea level was probably 6–9 m higher than present (Dutton et al., 2015) and average global sea surface temperature (SST) was estimated to be 0.5 ± 0.3 °C warmer relative to pre-industrial (PI) conditions (Hoffman et al., 2017). This temperature anomaly is associated with the Earth's orbital configuration, mostly related to changes in eccentricity and precession, which resulted in a high positive boreal summer insolation anomaly during the LIG relative to modern conditions (Otto-Bliesner et al., 2013; Otto-Bliesner et al., 2017). The positive LIG insolation anomaly was present between 90°N to 60°S during boreal summer months and resulted in enhanced (reduced) seasonality in the Northern (Southern) Hemisphere (Otto-Bliesner et al., 2021).

The positive LIG-PI temperature anomaly presents marked spatial variability, with particularly large anomalies in extratropical regions (Hoffman et al., 2017; Capron et al., 2017; Capron et al., 2014; Turney and Jones, 2010; McKay et al., 2011). In contrast, SST records suggest a slight cooling in tropical latitudes during the LIG relative to PI (Hoffman et al., 2017). These regional SST anomalies are supported by model simulations from the recent *lig127k* experiment performed as part of the fourth phase of the Paleoclimate Modelling Intercomparison Project (PMIP4) (Otto-Bliesner et al., 2021; Otto-Bliesner et al., 2020).

However, in some regions such as parts of the tropical Atlantic, the LIG is poorly documented with appropriate SST records due to the scarcity of long sediment cores with adequate high sedimentation rates.

* Corresponding author.
E-mail address: rodrigoan@id.uff.br (R.A. Nascimento).

https://doi.org/10.1016/j.gloplacha.2022.103889
Received 14 March 2022; Received in revised form 17 June 2022; Accepted 5 July 2022
Available online 9 July 2022

Most of tropical SST reconstructions used in LIG surface temperature compilations were derived from the almost 30 years old CLIMAP project (CLIMAP Project Members, 1984). The CLIMAP SST reconstructions were based on transfer function methods using microfossil assemblages, many of them with low temporal resolution. Accordingly, high resolution tropical SST records based on alternative proxies (e.g., Mg/Ca) can help to constrain the LIG SST evolution of this latitudinal band and provide relevant information from a period when the global average temperature was similar or higher than modern days. In this study, we present a new submillennial-resolution Mg/Ca-based LIG SST record from a marine sediment core retrieved from the western tropical South Atlantic (WTSA). We compare our LIG SST with instrumental PI SST from the Hadley Center of Sea Ice and Sea Surface temperature (HadISST1.1) data set (Rayner et al., 2003) for the time period 1871–1889 CE and with Mg/Ca-based Holocene SST values derived from the same sediment core investigated in the present study (Santos et al., 2022). Our results give support to a warmer LIG in the WTSA. We suggest that the retreat of polar sea ice during the LIG has the potential to warm tropical latitudes. Finally, we discuss the disagreement between proxy and PMIP model simulations.

2. Regional setting

Our study site is located in the northernmost part of the South Atlantic Subtropical Gyre (SASG) (Fig. 1). This region is marked by the bifurcation of the South Equatorial Current (SEC) between 10 and 14°S (Rodrigues et al., 2007), and forms the southward flowing Brazil Current (BC) and northward flowing North Brazil Under Current (NBUC)/North Brazil Current (NBC) (Stramma and England, 1999). This northward flow is ultimately responsible for the interhemispheric northward transport of water and heat in the Atlantic (Zhang et al., 2011; Lumpkin and Speer, 2003). The modern annual average SST in our study region is 27.5 °C with a seasonal range of 1.3 °C (Locarnini et al., 2018).

3. Methods

3.1. Sediment core

We investigated sediment core GL-1180, collected at the Brazilian tropical continental margin (8° 27′18“ S, 33° 32’53” W, 1037 m water depth). This core was provided by the Brazilian oil company Petrobras. The sediment core is 1732 cm long and was sampled at 2 cm resolution between centimeters 792 and 864. Sediment samples (~10 cm^3) were washed over a 63 μm sieve. The retained material was dried in an oven at 50 °C for 24 h and stored in acrylic containers.

3.2. Age model

A first age model for sediment core GL-1180 was published by Nascimento et al. (2021). It was based on six radiocarbon ages calibrated using the IntCal13 calibration curve (Reimer et al., 2013) with a reservoir effect of 400 ± 200 years, as well as the alignment of the GL-1180 benthic $\delta^{18}O$ record with the global $\delta^{18}O$ stack LR04 (Lisiecki and Raymo, 2005). Here we use a revised age model aimed at improving age control for the LIG. We also improved the age model for the Holocene portion of GL-1180 by the addition of two new radiocarbon ages.

For the LIG period, the revised age model is now based on the visual alignment of the benthic $\delta^{18}O$ record from core GL-1180 of *Cibicidoides* spp. (Nascimento et al., 2021) against the regional $\delta^{18}O$ stack (LS16) for the South Atlantic intermediate waters (Fig. S1 and Table S1) published by Lisiecki and Stern (2016). Alignment uncertainties were calculated following Govin et al. (2015). The LS16 regional stack has a resolution of 0.5 kyr, and the uncertainty for the period ranges from 2 to 3 kyr, while the LR04 has a resolution of 1 kyr and an uncertainty of 4 kyr. Accordingly, by using the LS16 we were able to reduce the alignment uncertainty from 4.3 to between 2.4 and 3.2 kyr.

For the Holocene, the revised age model is based on 5 radiocarbon ages (Table S1). Each radiocarbon age is based on 6 to 10 mg of *Globigerinoides ruber* and *Trilobatus sacculifer* shells from the size fraction larger than 150 μm. Analyses were performed at the Beta Analytic Radiocarbon Dating Laboratory (Miami, USA) using accelerator mass spectrometry. Besides including two new radiocarbon dates, a novelty of this age model was that we calibrated the radiocarbon ages against the most recent Marine20 calibration curve (Heaton et al., 2020). No additional reservoir effect was applied. Compared with earlier versions, Marine20 includes more realistic carbon cycle changes over the last 55 kyr and takes into account a rigorous time-dependent uncertainty of atmospheric $\Delta^{14}C$ (Heaton et al., 2020). The final age models for the two time intervals (Fig. S2 and S3) were built using the software Bacon v 2.3 (Blaauw and Christen, 2011).

3.3. Mg/Ca analyses

For Mg/Ca analyses, 20 shells of the surface-dwelling *G. ruber* (white, 250–300 μm) were handpicked from each core sample. *Globigerinoides ruber* (white) shows a preference for warm waters, ranging from tropical to subtropical latitudes (Kucera, 2007; Žarić et al., 2005). *Globigerinoides ruber* (white) dwells within the mixed layer of the WTSA (Nascimento

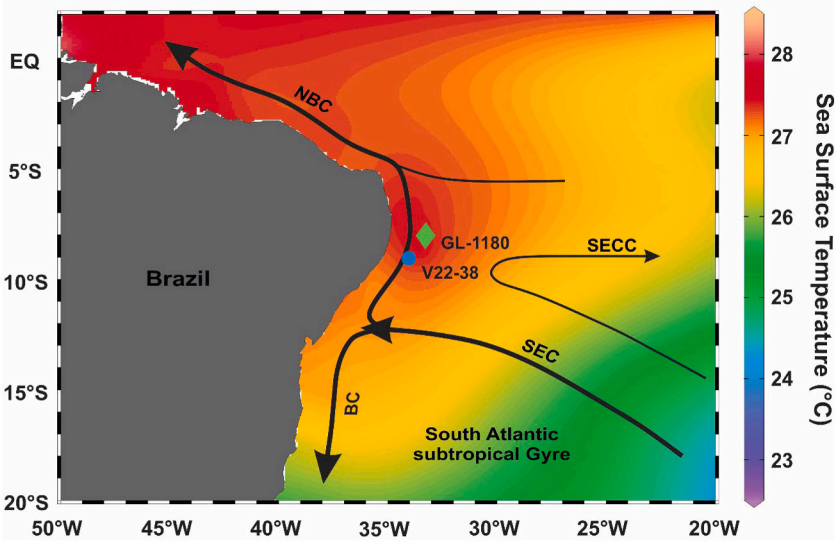

Fig. 1. Location of marine sediment core GL-1180 (green diamond). The blue circle indicates the location of marine sediment core V22–38 (CLIMAP Project Members, 1984). The colour scale depicts modern (1955–2017) mean annual sea surface temperature (Locarnini et al., 2018). Black arrows depict the schematic surface ocean circulation; BC: Brazil Current; NBC: North Brazil Current; SEC: South Equatorial Current; SECC: South Equatorial Countercurrent. The figure was partially generated using the software Ocean Data View (Schlitzer, 2017). (For interpretation of the references to colour in this figure legend, the reader is referred to the web version of this article.)

et al., 2021; Venancio et al., 2018). Although sediment trap samples from the subtropical western South Atlantic point to higher *G. ruber* (white) flux during summer conditions (Venancio et al., 2017), sediment traps from three moorings located near our core site (Žarić et al., 2005) indicate no seasonal variation in the flux of this species to the seafloor due to the low seasonal SST variability in the tropical Atlantic (Jonkers and Kučera, 2015). These results from sediment traps are consistent with a global planktonic foraminifera model (Fraile et al., 2009). In this model, *G. ruber* (white) signal is biased toward summer conditions at mid-latitudes, but, in the tropics, they represent annual average SST conditions.

The cleaning protocol of the *G. ruber* shells followed Barker et al. (2003). This is the same protocol used by Santos et al. (2022) for the analysis of Mg/Ca in *G. ruber* shells of sediment core GL-1180 over the last 24 kyr. Briefly, each sample was cleaned with water, methanol, and a hot hydrogen peroxide solution, with no reductive cleaning step. After cleaning, samples were dissolved in diluted HNO_3. Mg/Ca analyses were performed at the MARUM-Center for Marine Environmental Sciences, University of Bremen, using an inductively coupled plasma optical emission spectrometer (ICP-OES) (Agilent Technologies, 700 Series) with an autosampler (ASX-520 Cetac). Three replicates were measured and averaged. In addition to Ca and Mg, we measured Fe, Mn, and Al to monitor the effectiveness of the cleaning procedure. The calibration series consisted of one blank and five multi-element standards containing between 20 and 80 ppm of Ca prepared from a mixed standard purchased from SCP Science, France (Mg/Ca of 4.17 mmol mol^{-1}). All samples were within the calibrated concentration range. An in-house standard (Mg/Ca = 2.96 mmol mol^{-1}), as well as the standards ECRM 752–1 (Bureau of Analysed Standards, Great Britain) and Reinstoff Nr. 3 (Bundesanstalt für Materialforschung und –Prüfung, Germany), were used to verify the accuracy of the measurements and to allow inter-laboratory comparison. The in-house standard was measured every five samples, while the commercial standards were measured four times during the batch of analyses. The standard deviations of the in-house standard, ERCM 752–1, and Reinstoff Nr. 3 in this batch of analyses were 0.01 mmol mol^{-1} (0.36%, $n = 127$), 0.02 mmol mol^{-1} (0.46%, $n = 8$), and 0.00 mmol mol^{-1} (0.0%, n = 8), respectively. The average Al/Ca, Mn/Ca, and Fe/Ca ratios were 0.06, 0.09, and 0.42 mmol mol^{-1}, respectively. Samples with Al/Ca ratio higher than 0.3 mmol mol^{-1} or having Mg/Ca values outside of the 4 σ of the mean (σ = 0.2 mmol mol^{-1}) were discarded (one out of 32 samples).

A global sediment trap calibration showed that Mg/Ca ratio from *G. ruber* (white) has a sensitivity of ~3% per salinity unit and ~ −8% per 0.1 pH unit (Gray et al., 2018). These values agree with a laboratory culture study of planktonic foraminifera (Gray and Evans, 2019). Accordingly, the temperature was calculated using the species-specific Mg/Ca-temperature equation of Gray and Evans (2019) for *G. ruber* (white) that corrects the effect of salinity and pH of seawater on Mg/Ca values. To account for the pH effect, we used the atmospheric CO_2 protocol, which uses past atmospheric CO_2 concentration derived from Antarctic ice cores (Gray and Evans, 2019). The mean 1σ and 2σ uncertainty for all SST estimates derived from the Mg/Ca-SST calibration

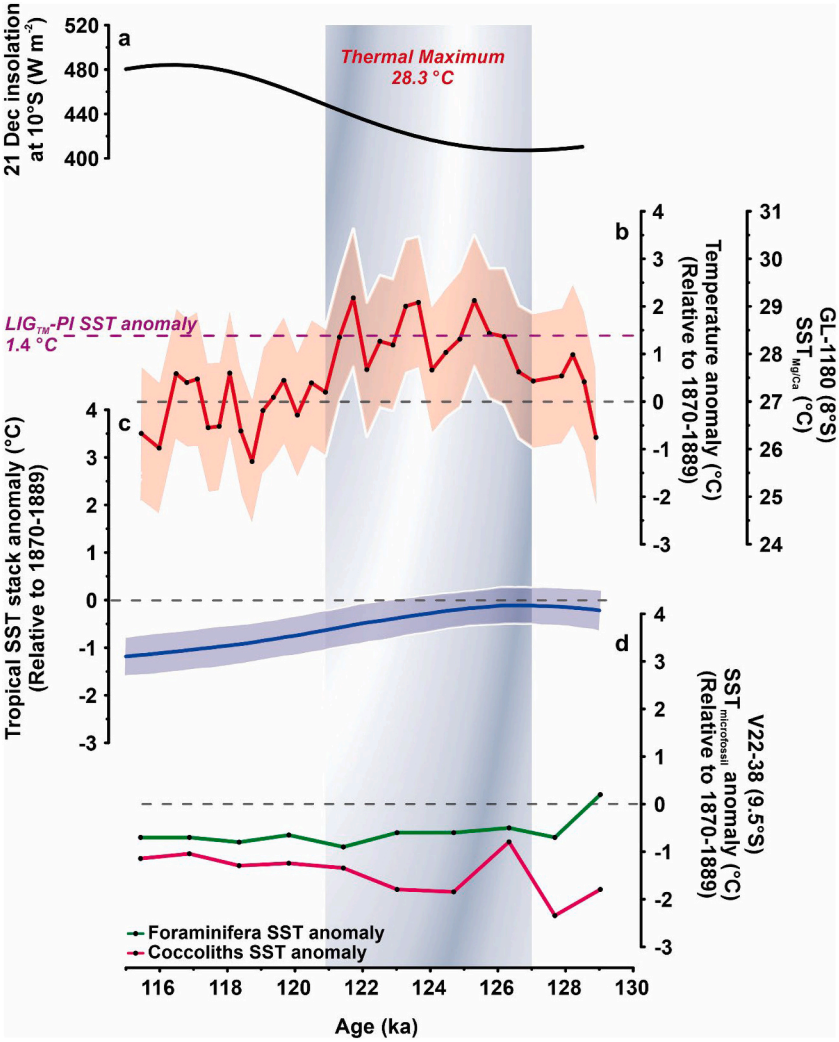

Fig. 2. Last Interglacial (LIG) sea surface temperature (SST) anomalies from the western tropical South Atlantic plotted against the tropical SST stack and insolation. a) 21st December insolation at 10°S for the LIG (Laskar et al., 2004). b) *Globigerinoides ruber* (white) Mg/Ca-based SST and SST anomaly relative to the pre-industrial (PI) from sediment core GL-1180 (this study). Mg/Ca SST records are presented with 2σ uncertainty (light red envelope). SST was estimated using the species-specific Mg/Ca-temperature equation for *G. ruber* from Gray and Evans (2019). c) Annual mean tropical SST anomaly (<23.5°N-S) within 2σ uncertainty (blue envelope) (Hoffman et al., 2017). d) Microfossil assemblage-derived annual mean SST anomaly relative to PI from sediment core V22–38 (9°S) (CLIMAP Project Members, 1984) as calculated by Hoffman et al. (2017). All anomalies were calculated relative to climatological PI (1870–1889) SST (Rayner et al., 2003). For cores GL-1180 and V22–28, we extracted the PI SST from the nearest grid cell. The dashed purple line in b indicates the average LIG thermal maximum SST (LIG_{TM}) relative to PI. The dashed black lines in b-d indicate the zero SST anomaly relative to PI. The gray vertical bar represents the LIG thermal maximum. (For interpretation of the references to colour in this figure legend, the reader is referred to the web version of this article.)

were 0.7 and 1.4 °C, respectively.

4. Results

Here, we present the first submillennial-scale resolution (i.e., ~0.4 ka between adjacent samples) foraminiferal Mg/Ca-based LIG SST record from the WTSA. The LIG SST record extends from ~129 to 115 ka (Fig. 2b). During this time, the Mg/Ca ratio ranges between 4.45 and 5.52 mmol mol^{-1} which gives calculated SSTs of between 25.6 and 29.1 °C. At 129 ka the SST was 26.1 °C increasing to 29 °C at 125 ka. Our data points to the LIG thermal maximum (LIG_{TM}) in the WTSA between ~127 and 121 ka, with an average SST of 28.3 ± 0.5 °C and SST maxima of 29.1 °C. At 121 ka, SST decreased to 26.8 ± 0.5 °C, indicating the end of the thermal maximum at site GL-1180. Between 121 and 116 ka the average SST was 26.9 ± 0.5 °C.

5. Discussion

5.1. *Globigerinoides ruber Mg/Ca as a proxy for western tropical South Atlantic SST*

The average Mg/Ca-based SST from the three uppermost GL-1180 core top samples (2 to 2.5 ka) (Santos et al., 2022) is 26.7 ± 0.0 °C. Importantly, the Mg/Ca-based Holocene SST from Santos et al. (2022) was recalculated on the revised age model using the same Mg/Ca-temperature equation applied in the present study (Fig. 3). The core top SST is in good agreement with the modern SST value of 26.9 °C extracted for 8°S and 33°W (the nearest grid cell to site GL-1180) from the HadISST1.1 data set (Rayner et al., 2003) for the period between 1870 and 1889, which we consider a reasonable approximation to PI conditions. Holocene surface temperature stacks (Kaufman et al., 2020; Marcott et al., 2013) and model simulations (Liu et al., 2014) show no expressive surface temperature differences between the Late Holocene (~2 ka) and PI in the tropics. Accordingly, the correspondence between SST from GL-1180 core top samples and PI suggests that our reconstruction is confidently representing the SST of the WTSA. Compared with modern SST value at the location of GL-1180, the core top SST is 0.8 °C lower than the annual average SST from the World Ocean Atlas 2018 (Locarnini et al., 2018), which can be attributed to the effect of the current global warming (Gulev et al., 2021).

5.2. *Proxy-based LIG SST evolution of the WTSA compared with the current interglacial*

To compare our LIG SST records with PI conditions we use the average LIG SST between 127 and 121 ka (LIG_{TM}), when our record exhibits maximum values (28.3 ± 0.5 °C), and the average climatological PI SST data from the HadISST1.1 data set (Rayner et al., 2003).

The LIG_{TM}-PI temperature difference indicates that the region of GL-1180 was 1.4 ± 0.4 °C warmer during the LIG relative to PI conditions (Fig. 2b). Given the stability of the WTSA mixed layer, this positive SST anomaly may point to a regional feature of the WTSA. Interestingly, such substantial positive anomaly contradicts, at least regionally, a recent global SST compilation showing that, in general, the tropical band (<23.5°N-S) was slightly colder during the LIG (at 125 ka) compared to PI times (Fig. 2c) (Hoffman et al., 2017). Most of the SST records compiled by Hoffman et al. (2017) are based on transfer functions using microfossil assemblages (75 out of 107). In the tropical Atlantic, from 26 LIG SST records, 3 are based on Mg/Ca and 4 on $U^{k'}_{37}$, while 19 records are derived from microfossil assemblages. However, microfossil assemblages resulted in systematically lower LIG SSTs than those estimated by geochemical proxies like Mg/Ca and alkenones unsaturation index ($U^{k'}_{37}$) (Hoffman et al., 2017). Indeed, LIG SST records derived from foraminiferal and coccoliths assemblages from site V22–38 (9°S) (CLIMAP members, 1984), located near core GL-1180 (Fig. 1), show a negative SST anomaly of up to ~2 °C between 128 and 121 ka relative to PI

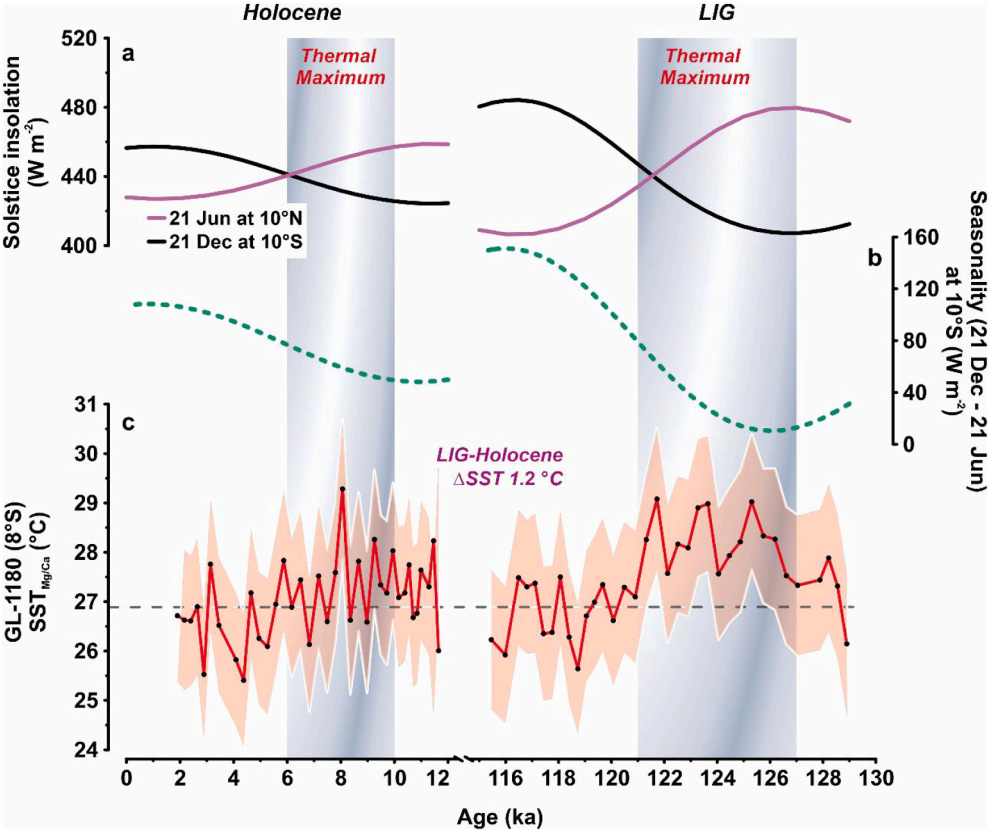

Fig. 3. Sea surface temperature (SST) reconstruction of the western tropical South Atlantic for the Last Interglacial (LIG) compared to the Holocene. a) Solstice insolation. Purple line depicts 21 June isolation at 10°N and black line depicts 21 December insolation at 10°S (Laskar et al., 2004). b) Dashed green line depicts insolation seasonality (21 Dec – 21 Jun) at 10°S (Laskar et al., 2004). c) *Globigerinoides ruber* Mg/Ca-based SST reconstructions for the LIG (this study) and the Holocene (on the revised Holocene age model) (Santos et al., 2022) from sediment core GL-1180. SST was estimated using the species-specific Mg/Ca-temperature equation for *G. ruber* from Gray and Evans (2019). Dashed black line indicates the climatological pre-industrial SST near site GL-1180 (Rayner et al., 2003). Mg/Ca SST records are presented with 2σ uncertainty as shown by the envelopes of the curves. The gray vertical bars represent the LIG and Holocene thermal maxima. (For interpretation of the references to colour in this figure legend, the reader is referred to the web version of this article.)

conditions (Fig. 2d). The contrast between our Mg/Ca-based LIG SST anomaly and transfer functions-based SST records from core V22–38 demonstrates the disagreement between proxy-based LIG SST reconstructions. Accordingly, the negative anomaly in the tropical SST stack from Hoffman et al. (2017) can be an artifact resulting from the averaging of proxy-based SST records, which were mostly based on microfossil assemblage transfer functions. Our results point to a spatial LIG SST variability within the tropical Atlantic, which can also be dampened by the averaging of SST records composed mostly by a single proxy. Ultimately, the disagreement between proxies for SST do not necessarily advocate against SST records derived from microfossil assemblages. Instead, they call for an better evaluation and understanding of these proxies in order to accurately constrain the evolution of the tropical Atlantic SST during the LIG.

We compare the LIG_{TM} with the average Holocene SST (between 2 and 10 ka; Fig. 3) from the same core (i.e., GL-1180) (Santos et al., 2022). WTSA SST was 1.2 ± 0.8 °C higher during the LIG relative to the Holocene. If we consider only the Holocene thermal maximum (6 to 10 ka), the positive LIG SST anomaly is 0.9 ± 0.7 °C. Meanwhile, the LIG SST anomaly relative to the late portion of the Holocene (2 to 5 ka) was 1.7 ± 0.7 °C. Although the 2σ error envelopes of the LIG and Holocene overlap each other (Fig. 3c), the use of the same proxy applied on the same foraminifera species allows us to suggest that the positive LIG-Holocene SST anomaly is a robust oceanographic feature of the WTSA.

Such a positive LIG-Holocene SST anomaly has been previously observed in tropical SST records and is thought to have been caused by the large magnitude of seasonal insolation changes during the LIG relative to the Holocene (Leduc et al., 2010). This explanation implies a seasonal bias in proxy-based SST toward boreal summer. Indeed, it has been suggested that most of the proxy-based SST records over the last two interglacial periods are biased toward the boreal summer/autumn insolation (Bova et al., 2021). Our SST record seems also to follow boreal summer insolation rather than local insolation (Fig. 3a, c). Qualitatively, such seasonal bias might explain our reconstructed positive LIG SST anomaly relative to the Holocene and PI.

In the southern tropics, the modern seasonal difference of incoming solar radiation (Dec 21 minus June 21) at 10°S (~100 W m^{-2}) is higher than that of the early Holocene (~50 W m^{-2}) and LIG thermal maximum (~20 W m^{-2}) (Fig. 3b), but the modern seasonal SST amplitude at site GL-1180 is only 1.3 °C (Locarnini et al., 2018). As the local incoming solar radiation plays the main role in controlling seasonal SST variations, we would expect the seasonality of the WTSA SST to be even lower during the LIG relative to the early Holocene and modern times. Indeed, at site V22–38 (Fig. 1), the seasonality of SST based on microfossil assemblage transfer function was estimated to be 1.6 °C for the LIG and 3 °C in core top sample (0–1 cm) (CLIMAP Members, 1984). Although this core top sample overestimates the modern seasonality around site V22–38, the results from CLIMAP support our reasoning that the WTSA reached the highest SST value of the last two interglacial periods when the seasonality of SST was at the lowest level. As our study area is not currently influenced by seasonal upwelling or turbulent mixing, these oceanographic processes are not expected to affect the seasonality of *G. ruber* shell flux at site GL-1180. Together with the arguments presented in Section 3.3, the low seasonality of insolation at the southern tropics during the LIG further suggests that our SST record is not seasonally biased and that the positive LIG SST anomaly is a consistent feature of the WTSA. However, by ruling out the effect of a seasonal bias, the cause of the positive LIG SST anomaly in the WTSA remains open.

5.3. Origin of recorded warmth during the LIG: Sea ice feedbacks on tropical SST

The sea ice-albedo feedback can play a major role in tropical SST during the LIG (Zhang and Chen, 2021). Many studies have used sensitivity model experiments to investigate the consequences of future Arctic sea ice loss on global climate by applying sea-ice scenarios of representative concentration pathway (RCP) 8.5 to coupled climate models (e.g., Wang et al., 2018; Sun et al., 2018; Tomas et al., 2016; Deser et al., 2015). These simulations show that sea ice loss results in a warming of the troposphere and ocean surface that extends into the tropics and advances toward the Southern Hemisphere. The projected warming pattern is symmetric at both sides of the equator and strikingly resembles the pattern for projected greenhouse gases (GHG)-forced global warming, albeit with a lower magnitude. The tropical surface waters warming due to Arctic sea ice loss can reach up to 0.3 °C (e.g., Deser et al., 2015). The role of future Arctic and Antarctic sea ice loss in tropical climate was investigated under RCP 8.5 sea ice loss scenario, with 70% and 35% Arctic summer and Antarctic winter sea ice loss, respectively (England et al., 2020). Similar to its northern counterpart, Antarctic sea ice retreat causes surface warming that extends into the tropics and advances toward the Northern Hemisphere. The combined effects of Arctic and Antarctic sea ice losses can account for up to 0.8 °C or 30% of the GHG-forced future tropical warming (England et al., 2020).

Studies have pointed to a reduced summer sea ice extent in the Arctic during the LIG relative to PI (e.g., Stein et al., 2017; Nørgaard-Pedersen et al., 2007; CAPE Members, 2006). An average of 16 climate model simulations in the PMIP4 pointed to an Arctic summer sea ice loss of 50% during the LIG relative to PI (Kageyama et al., 2021). Using a fully coupled climate model with improved sea ice physics, Guarino et al. (2020) simulated a complete summer sea ice loss in the Arctic during the LIG. In the Southern Ocean, winter sea ice was estimated to have retreated by 65% during the LIG relative to PI (Holloway et al., 2016). Spatially resolved winter sea ice losses are 67, 59, and 43% in the Atlantic, Indian, and Pacific sectors of the Southern Ocean, respectively (Holloway et al., 2017). The Antarctic sea ice retreat is corroborated by the lower flux of sea salt sodium in Antarctic ice core Dome C during the LIG relative to the Holocene (Wolff et al., 2006). Therefore, we argue that the internal climate feedback associated with the polar sea ice retreat during the LIG could explain a tropical LIG-PI and LIG-Holocene positive SST anomaly of about 1 °C, as shown herewith.

5.4. Proxy-based LIG-PI anomaly versus PMIP4 simulations

Climate models in PMIP4 simulate negative LIG SST anomalies in tropical latitudes (Otto-Bliesner et al., 2021). We concentrate on the subset from experiment *lig127k* performed by 6 climate models (Table S3) to explore the differences between model simulation and proxy results, focusing on the site GL-1180. Experiment *lig127k* represents the time slice of 127 ka (Otto-Bliesner et al., 2017) and was compared with experiment *piControl*, that simulates PI conditions (Eyring et al., 2016). The main difference between *piControl* and *lig127k* experiments is the latitudinal and seasonal distribution of insolation (Otto-Bliesner et al., 2017).

Although each model shows a different pattern of SST anomaly (Fig. S4), the *lig127k* model ensemble exhibits a negative annual mean SST anomaly of up to 1 °C in the tropical and South Atlantic relative to the *piControl* run (Fig. 4). This result agrees with an ensemble of 17 climate models participating in PMIP4 simulations (Otto-Bliesner et al., 2021). At the location of site GL-1180, the ensemble annual average anomaly from the 6 climate models examined in this study was −0.4 ± 0.3 °C. Seasonal LIG SST anomaly shows a negligible positive anomaly during the austral winter (~0.1 °C) and a negative anomaly of up to 1.5 °C during the austral summer (Fig. S5 and S6). This seasonal analysis indicates that the negative annual average LIG SST anomaly in WTSA, as simulated by experiment *lig127k*, is forced by the low insolation in the Southern Hemisphere during austral summer (boreal winter).

The occurrence of proxy-model inconsistencies for LIG SST reconstructions has been previously observed and investigated (e.g., Bakker et al., 2014; Bakker and Renssen, 2014; Otto-Bliesner et al., 2013). These inconsistencies can arise from both, proxy and model simulations. Starting with proxy data, Mg/Ca from planktonic

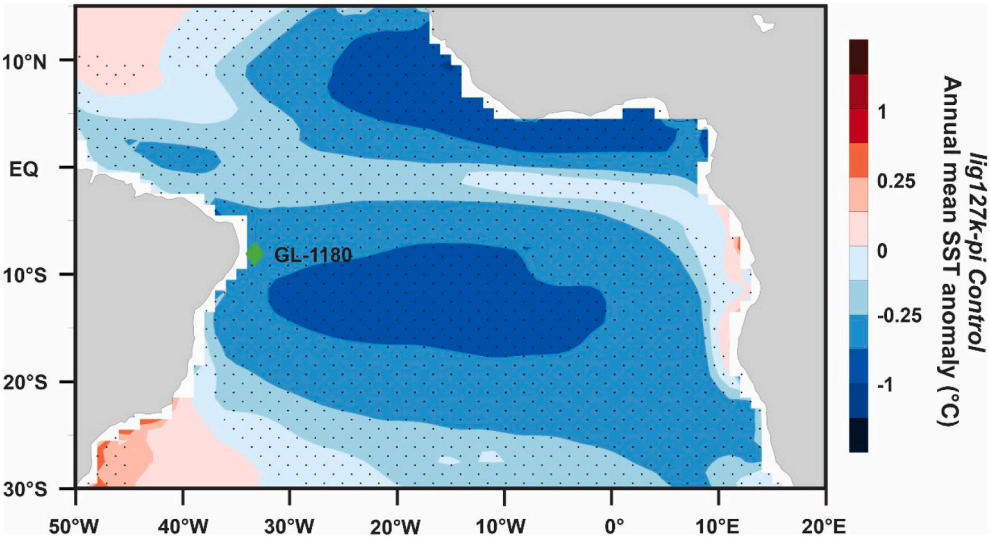

Fig. 4. Annual mean sea surface temperature (SST) anomaly calculated between the Last Interglacial (LIG) and the pre-industrial (PI) (i.e., LIG-PI) from an ensemble of six climate model simulations (Table S3) from experiments *lig127k* and *piControl* as part of the Paleoclimate Modelling Intercomparison Project 4. The green diamond indicates the location of marine sediment core GL-1180. Stippling represents areas where at least four of the six models (i.e., 67%) agree with the signal of the change. Note that the colour scale is not linear. (For interpretation of the references to colour in this figure legend, the reader is referred to the web version of this article.)

foraminifera may reflect a more local instead of broader oceanographic features and/or may be biased toward the warm season (e.g., Leduc et al., 2010; Lohmann et al., 2013; Bakker and Renssen, 2014; Schneider et al., 2010). The basic assumption when using planktonic foraminiferal shells as climate archives is that the environmental conditions determining calcification depth, seasonal preferences, and preservation have been invariant over the covered period. As discussed in Section 5.2, the low seasonal variation in the southern tropics during the LIG (Fig. 3b) makes it very unlikely that our SST reconstruction is seasonally biased (Jonkers and Kučera, 2015, 2017). Meanwhile, the absence of local oceanographic processes, such as seasonal upwelling, around site GL-1180 indicates that the LIG SST anomaly does not result from a local oceanographic feature. However, despite the lack of substantial evidence, we cannot rule out that subtle environmental changes were sufficient to create a warm-season bias or a change in depth habitat in LIG foraminifera.

On the other hand, climate models may oversimplify important internal feedbacks of the climate system acting during the LIG (Bakker et al., 2014; Bakker et al., 2013). The lack of internal feedbacks is even more relevant for equilibrium simulations, as performed in the *lig127k* experiment. Indeed, the *lig127k* does not capture the diversity of transient forcings and feedbacks setting the LIG climate, as for example, climate change driven by nonlinear interplay of ice-sheet–ocean coupling (Otto-Bliesner et al., 2017). Therefore, the absence of important internal climate feedbacks can lead the simulations to artificially reproduce a climate system controlled mostly by orbital forcing (Zhang and Chen, 2021). Additionally, a major uncertainty of experiment *lig127k* is that it uses the modern ice-sheet geometry as boundary condition (Otto-Bliesner et al., 2017). However, the sea level was estimated to be between 6 and 9 m higher during the LIG relative to modern (Dutton et al., 2015), indicating reduced ice-sheet volume relative to current times. Indeed, the presence of remnant continental ice from the preceding glacial appears to play an important role on the LIG SST evolution (Capron et al., 2017; Bakker et al., 2013).

Since interglacial climate evolution seems to depend on the preceding deglaciation (Barker et al., 2019), future numeric experiments with transient simulations of the penultimate deglaciation and LIG will help to constrain the evolution of LIG SST in the tropics (e.g., Menviel et al., 2019). The data presented here will be useful as a validation target for climate models (Otto-Bliesner et al., 2021).

6. Conclusions

Here, we presented a new submillennial-resolution Mg/Ca-based LIG SST record from the WTSA. We found that the LIG was warmer by 1.4 ± 0.4 and 1.2 ± 0.8 °C than pre-industrial and Holocene conditions, respectively. These results indicate spatial variability of tropical LIG SST rather than a predominantly colder LIG relative to the pre-industrial. We show that a positive tropical LIG SST anomaly could be explained by polar sea ice retreat during the LIG, which warms surface waters all the way into the tropics. The disagreement between LIG SST anomalies from PMIP4 simulations and our record can result from: (i) changes in the ecological behavior of planktonic foraminifera over the geological past; (ii) imprecise boundary conditions (e.g., ice sheets) and limitations in capturing internal Earth's climate feedbacks can lead numeric model experiments to produce inaccurate SST. Identifying whether this positive anomaly in the WTSA is consistent and a widespread feature of tropical latitudes requires increasing the accuracy of proxy-based SST reconstructions and more records. Additionally, transient simulations of the penultimate deglaciation and LIG can help to capture the feedbacks in Earth's climate system that led to LIG SST evolution. Our study provides a new validation target for climate models, which is crucial in view of the current simulations from PMIP4.

Declaration of Competing Interest

The authors declare that they have no known competing financial interests or personal relationships that could have appeared to influence the work reported in this paper.

Acknowledgments

We thank two anonymous reviewers for their constructive suggestions that substantially improved our manuscript. We thank the Petrobras for providing the sediment core used in this study. This study was supported by the CAPES-ASpECTO project (grant 88887.091731/2014-01) CNPq-Aspecto (grant 429767/2018-8), CAPES-PRINT CLIMATE Project (grant 88887.310301/2018-00) and CNPq Project RAiN (grant 406322/2018-0). R.A.N. acknowledges the scholarship from CAPES (grant 88887.176103/2018-00). I.M.V acknowledges the scholarship from CAPES (grant 88881.512929/2020-01) and the Alexander von Humboldt Foundation. C.M.C. acknowledges the financial support from FAPESP (grants 2018/15123-4 and 2019/24349-9), CAPES (grant 88881.313535/2019-01), CNPq (grant 312458/2020-7), and the Alexander von Humboldt Foundation. A.L.S.A. is a senior scholar CNPq (grant 302521/2017-8). A.G. acknowledges the financial support from ANR (grant ANR-18-BELM-0001-06). We also acknowledge the partial support from the Coordenação de Aperfeiçoamento de Pessoal de Nível

Superior – Brasil (CAPES) – Finance Code 001. This is LSCE publication number 8013. All data presented in this manuscript are available at www.pangaea.de.

Appendix A. Supplementary data

Supplementary data to this article can be found online at https://doi.org/10.1016/j.gloplacha.2022.103889.

References

Bakker, P., Renssen, H., 2014. Last interglacial model–data mismatch of thermal maximum temperatures partially explained. Clim. Past 10 (4), 1633–1644. https://doi.org/10.5194/cp-10-1633-2014.

Bakker, P., Stone, E.J., Charbit, S., Gröger, M., Krebs-Kanzow, U., Ritz, S.P., Varma, V., Khon, V., Lunt, D.J., Mikolajewicz, U., Prange, M., 2013. Last interglacial temperature evolution–a model inter-comparison. Clim. Past 9 (2), 605–619. https://doi.org/10.5194/cp-9-605-2013.

Bakker, P., Masson-Delmotte, V., Martrat, B., Charbit, S., Renssen, H., Gröger, M., Krebs-Kanzow, U., Lohmann, G., Lunt, D.J., Pfeiffer, M., Phipps, S.J., 2014. Temperature trends during the present and last Interglacial periods–a multi-model-data comparison. Quat. Sci. Rev. 99, 224–243. https://doi.org/10.1016/j.quascirev.2014.06.031.

Barker, S., Greaves, M., Elderfield, H., 2003. A study of cleaning procedures used for foraminiferal Mg/Ca paleothermometry. Geochem. Geophys. Geosyst. 4 (9), 1–20. https://doi.org/10.1029/2003GC000559.

Barker, S., Knorr, G., Conn, S., Lordsmith, S., Newman, D., Thornalley, D., 2019. Early interglacial legacy of deglacial climate instability. Paleoceanogr. Paleoclim. 34 (8), 1455–1475. https://doi.org/10.1029/2019PA003661.

Blaauw, M., Christen, J.A., 2011. Flexible paleoclimate age-depth models using an autoregressive gamma process. Bayesian Anal. 6 (3), 457–474. https://doi.org/10.1214/11-BA618.

Bova, S., Rosenthal, Y., Liu, Z., Godad, S.P., Yan, M., 2021. Seasonal origin of the thermal maxima at the Holocene and the last interglacial. Nature 589 (7843), 548–553. https://doi.org/10.1038/s41586-020-03155-x.

Capron, E., Govin, A., Stone, E.J., Masson-Delmotte, V., Mulitza, S., Otto-Bliesner, B., Rasmussen, T.L., Sime, L.C., Waelbroeck, C., Wolff, E.W., 2014. Temporal and spatial structure of multi-millennial temperature changes at high latitudes during the last interglacial. Quat. Sci. Rev. 103, 116–133. https://doi.org/10.1016/j.quascirev.2014.08.018.

Capron, E., Govin, A., Feng, R., Otto-Bliesner, B.L., Wolff, E.W., 2017. Critical evaluation of climate syntheses to benchmark CMIP6/PMIP4 127 ka last Interglacial simulations in the high latitude regions. Quat. Sci. Rev. 168, 137–150. https://doi.org/10.1016/j.quascirev.2017.04.019.

CLIMAP Project Members, 1984. The last Interglacial Ocean. Quat. Res. 21, 123–224. https://doi.org/10.1016/0033-5894(84)90098-X.

Deser, C., Tomas, R.A., Sun, L., 2015. The role of ocean–atmosphere coupling in the zonal-mean atmospheric response to Arctic Sea ice loss. J. Clim. 28 (6), 2168–2186. https://doi.org/10.1175/JCLI-D-14-00325.1.

Dutton, A., Carlson, A.E., Long, A.J., Milne, G.A., Clark, P.U., DeConto, R., Horton, B.P., Rahmstorf, S., Raymo, M.E., 2015. Sea-level rise due to polar ice-sheet mass loss during past warm periods. Science 349 (6244), aaa4019. https://doi.org/10.1126/science.aaa4019.

England, M.R., Polvani, L.M., Sun, L., Deser, C., 2020. Tropical climate responses to projected Arctic and Antarctic Sea-ice loss. Nat. Geosci. 13 (4), 275–281. https://doi.org/10.1038/s41561-020-0546-9.

Eyring, V., Bony, S., Meehl, G.A., Senior, C.A., Stevens, B., Stouffer, R.J., Taylor, K.E., 2016. Overview of the coupled Model Intercomparison Project phase 6 (CMIP6) experimental design and organization. Geosci. Model Dev. 9, 1937–1958. https://doi.org/10.5194/gmd-9-1937-2016.

Fraile, I., Mulitza, S., Schulz, M., 2009. Modeling planktonic foraminiferal seasonality: Implications for sea-surface temperature reconstructions. Mar. Micropaleontol. 72 (1–2), 1–9. https://doi.org/10.1016/j.marmicro.2009.01.003.

Govin, A., Capron, E., Tzedakis, P.C., Verheyden, S., Ghaleb, B., Hillaire-Marcel, C., et al., 2015. Sequence of events from the onset to the demise of the last Interglacial: evaluating strengths and limitations of chronologies used in climatic archives. Quat. Sci. Rev. 129, 1–36. https://doi.org/10.1016/j.quascirev.2015.09.018.

Gray, W.R., Evans, D., 2019. Nonthermal Influences on Mg/Ca in Planktonic Foraminifera: a Review of Culture Studies and Application to the last Glacial Maximum. Paleoceanogr. Paleoclim. 34, 306–315. https://doi.org/10.1029/2018PA003517.

Gray, W.R., Weldeab, S., Lea, D.W., Rosenthal, Y., Gruber, N., Donner, B., Fischer, G., 2018. The effects of temperature, salinity, and the carbonate system on Mg/Ca in Globigerinoides ruber (white): a global sediment trap calibration. Earth Planet. Sci. Lett. 482, 607–620. https://doi.org/10.1016/j.epsl.2017.11.026.

Guarino, M.V., Sime, L.C., Schröeder, D., Malmierca-Vallet, I., Rosenblum, E., Ringer, M., Ridley, J., Feltham, D., Bitz, C., Steig, E.J., Wolff, E., 2020. Sea-ice-free Arctic during the last Interglacial supports fast future loss. Nat. Clim. Chang. 10 (10), 928–932. https://doi.org/10.1038/s41558-020-0865-2.

Gulev, S.K., Thorne, P.W., Ahn, J., Dentener, F.J., Domingues, C.M., Gerland, S., Gong, D., Kaufman, D.S., Nnamchi, H.C., Quaas, J., Rivera, J.A., Sathyendranath, S., Smith, S.L., Trewin, B., von Shuckmann, K., Vose, R.S., 2021. Changing state of the climate system. In: Masson-Delmotte, V., Zhai, P., Pirani, A., Connors, S.L., Péan, C., Berger, S., Caud, N., Chen, Y., Goldfarb, L., Gomis, M.I., Huang, M., Leitzell, K., Lonnoy, E., Matthews, J.B.R., Maycock, T.K., Waterfield, T., Yelekçi, O., Yu, R., Zhou, B. (Eds.), Climate Change 2021: The Physical Science Basis. Contribution of Working Group I to the Sixth Assessment Report of the Intergovernmental Panel on climate Change. Cambridge University Press (In Press).

Heaton, T.J., Köhler, P., Butzin, M., Bard, E., Reimer, R.W., Austin, W.E.N., Bronk Ramsey, C., Grootes, P.M., Hughen, K.A., Kromer, B., Reimer, P.J., Adkins, J., Burke, A., Cook, M.S., Olsen, J., Skinner, L.C., 2020. Marine20 - the Marine Radiocarbon Age Calibration Curve (0-55,000 cal BP). Radiocarbon 62, 779–820. https://doi.org/10.1017/RDC.2020.68.

Hoffman, J.S., Clark, P.U., Parnell, A.C., He, F., 2017. Regional and global sea-surface temperatures during the last interglaciation. Science 355, 276–279. https://doi.org/10.1126/science.aai8464.

Holloway, M.D., Sime, L.C., Singarayer, J.S., Tindall, J.C., Bunch, P., Valdes, P.J., 2016. Antarctic last interglacial isotope peak in response to sea ice retreat not ice-sheet collapse. Nat. Commun. 7 (1), 1–9. https://doi.org/10.1038/ncomms12293.

Holloway, M.D., Sime, L.C., Allen, C.S., Hillenbrand, C.D., Bunch, P., Wolff, E., Valdes, P.J., 2017. The spatial structure of the 128 ka Antarctic Sea ice minimum. Geophys. Res. Lett. 44 (21), 11–129. https://doi.org/10.1002/2017GL074594.

Jonkers, L., Kučera, M., 2015. Global analysis of seasonality in the shell flux of extant planktonic Foraminifera. Biogeosciences 12 (7), 2207–2226. https://doi.org/10.5194/bg-12-2207-2015.

Jonkers, L., Kučera, M., 2017. Quantifying the effect of seasonal and vertical habitat tracking on planktonic foraminifera proxies. Clim. Past 13 (6), 573–586. https://doi.org/10.5194/cp-13-573-2017.

Kageyama, M., Braconnot, P., Harrison, S.P., Haywood, A.M., Jungclaus, J., Otto-Bliesner, B.L., Peterschmitt, J.Y., Abe-Ouchi, A., Albani, S., Bartlein, P.J., Brierley, C., 2018. PMIP4-CMIP6: the contribution of the Paleoclimate Modelling Intercomparison Project to CMIP6. Geosci. Model Dev. Discuss. 11 (3), 1033–1057. https://doi.org/10.5194/gmd-2016-106.

Kageyama, M., Sime, L.C., Sicard, M., Guarino, M.V., de Vernal, A., Stein, R., Schroeder, D., Malmierca-Vallet, I., Abe-Ouchi, A., Bitz, C., Braconnot, P., 2021. A multi-model CMIP6-PMIP4 study of Arctic Sea ice at 127 ka: sea ice data compilation and model differences. Clim. Past 17 (1), 37–62. https://doi.org/10.5194/cp-17-37-2021.

Kaufman, D., McKay, N., Routson, C., Erb, M., Davis, B., Heiri, O., Jaccard, S., et al., 2020. A global database of Holocene paleotemperature records. Sci. Data 7, 1–34. https://doi.org/10.1038/s41597-020-0445-3.

Kucera, M., 2007. Chapter six planktonic foraminifera as tracers of past oceanic environments. Dev. Mar. Geol. 1, 213–262. https://doi.org/10.1016/S1572-5480(07)01011-1.

Laskar, J., Robutel, P., Joutel, F., Gastineau, M., Correia, A.C.M., Levrard, B., 2004. A long-term numerical solution for the insolation quantities of the Earth. Astron. Astrophys. 428, 261–285. https://doi.org/10.1051/0004-6361:20041335.

Leduc, G., Schneider, R., Kim, J.H., Lohmann, G., 2010. Holocene and Eemian Sea surface temperature trends as revealed by alkenone and Mg/Ca paleothermometry. Quat. Sci. Rev. 29 (7–8), 989–1004. https://doi.org/10.1016/j.quascirev.2010.01.004.

Lisiecki, L.E., Raymo, M.E., 2005. A Pliocene-Pleistocene stack of 57 globally distributed benthic $\delta^{18}O$ records. Paleoceanography 20 (1), 1–17. https://doi.org/10.1029/2004PA001071.

Lisiecki, L.E., Stern, J.V., 2016. Regional and global benthic δ18O stacks for the last glacial cycle. Paleoceanography 31, 1368–1394. https://doi.org/10.1002/2016PA003002.

Liu, Z., Zhu, J., Rosenthal, Y., Zhang, X., Otto-Bliesner, B.L., Timmermann, A., Smith, R. S., Lohmann, G., Zheng, W., Timm, O.E., 2014. The Holocene temperature conundrum. Proc. Natl. Acad. Sci. 111 (34), E3501–E3505. https://doi.org/10.1073/pnas.1407229111.

Locarnini, R.A., Mishonov, A.V., Baranova, O.K., Boyer, T.P., Zweng, M.M., Garcia, H.E., Reagan, J.R., Seidov, D., Weathers, K., Paver, C.R., Smolyar, I., 2018. World ocean atlas 2018. In: Mishonov Technical, A. (Ed.), Temperature, vol. 1. NOAA Atlas NESDIS 81, 52pp.

Lohmann, G., Pfeiffer, M., Laepple, T., Leduc, G., Kim, J.H., 2013. A model–data comparison of the Holocene global sea surface temperature evolution. Clim. Past 9 (4), 1807–1839. https://doi.org/10.5194/cp-9-1807-2013.

Lumpkin, R., Speer, K., 2003. Large-scale vertical and horizontal circulation in the North Atlantic Ocean. J. Phys. Oceanogr. 33, 1902–1920. https://doi.org/10.1175/1520-0485(2003)033%3C1902:LVAHCI%3E2.0.CO;2.

Marcott, S.A., Shakun, J.D., Clark, P.U., Mix, A.C., 2013. A reconstruction of regional and global temperature for the past 11,300 years. Science 339, 1198–1201. https://doi.org/10.1126/science.1228026.

McKay, N.P., Overpeck, J.T., Otto-Bliesner, B.L., 2011. The role of ocean thermal expansion in last Interglacial Sea level rise. Geophys. Res. Lett. 38, 4–9. https://doi.org/10.1029/2011GL048280.

Members, C.A.P.E., 2006. Last Interglacial Arctic warmth confirms polar amplification of climate change. Quat. Sci. Rev. 25 (13–14), 1383–1400. https://doi.org/10.1016/j.quascirev.2006.01.033.

Menviel, L., Capron, E., Govin, A., Dutton, A., Tarasov, L., Abe-Ouchi, A., Drysdale, R.N., Gibbard, P.L., Gregoire, L., He, F., Ivanovic, R.F., 2019. The penultimate deglaciation: protocol for Paleoclimate Modelling Intercomparison Project (PMIP) phase 4 transient numerical simulations between 140 and 127 ka, version 1.0. Geosci. Model Dev. 12 (8), 3649–3685. https://doi.org/10.5194/gmd-12-3649-2019.

Nascimento, R.A., Venancio, I.M., Chiessi, C.M., Ballalai, J.M., Kuhnert, H., Johnstone, H., Santos, T.P., Prange, M., Govin, A., Crivellari, S., Mulitza, S., Albuquerque, A.L.S., 2021. Tropical Atlantic stratification response to late

Quaternary precessional forcing. Earth Planet. Sci. Lett. 568, 117030. https://doi.org/10.1016/j.epsl.2021.117030.
Nørgaard-Pedersen, N., Mikkelsen, N., Lassen, S.J., Kristoffersen, Y., Sheldon, E., 2007. Reduced Sea ice concentrations in the Arctic Ocean during the last interglacial period revealed by sediment cores off northern Greenland. Paleoceanography 22 (1). https://doi.org/10.1029/2006PA001283.
Otto-Bliesner, B.L., Rosenbloom, N., Stone, E.J., Mckay, N.P., Lunt, D.J., Brady, E.C., Overpeck, J.T., 2013. How warm was the last interglacial? New model-data comparisons. Philos. Trans. R. Soc. A Math. Phys. Eng. Sci. 371 https://doi.org/10.1098/rsta.2013.0097.
Otto-Bliesner, B.L., Braconnot, P., Harrison, S.P., Lunt, D.J., Abe-Ouchi, A., Albani, S., Bartlein, P.J., Capron, E., Carlson, A.E., Dutton, A., Fischer, H., Goelzer, H., Govin, A., Haywood, A., Joos, F., Legrande, A.N., Lipscomb, W.H., Lohmann, G., Mahowald, N., Nehrbass-Ahles, C., Pausata, F.S.R., Peterschmitt, J.Y., Phipps, S.J., Renssen, H., Zhang, Q., 2017. The PMIP4 contribution to CMIP6 - part 2: two interglacials, scientific objective and experimental design for Holocene and last Interglacial simulations. Geosci. Model Dev. 10, 3979–4003. https://doi.org/10.5194/gmd-10-3979-2017.
Otto-Bliesner, B.L., Brady, E.C., Tomas, R.A., Albani, S., Bartlein, P.J., Mahowald, N.M., Shafer, S.L., Kluzek, E., Lawrence, P.J., Leguy, G., Rothstein, M., Sommers, A.N., 2020. A Comparison of the CMIP6 midHolocene and lig127k Simulations in CESM2. Paleoceanogr. Paleoclim. 35 https://doi.org/10.1029/2020PA003957.
Otto-Bliesner, B.L., Brady, E.C., Zhao, A., Brierley, C.M., Axford, Y., Capron, E., Govin, A., Hoffman, J.S., Isaacs, E., Kageyama, M., Scussolini, P., Tzedakis, P.C., Williams, C.J.R., Wolff, E., Abe-Ouchi, A., Braconnot, P., Ramos Buarque, S., Cao, J., De Vernal, A., Vittoria Guarino, M., Guo, C., Legrande, A.N., Lohmann, G., Meissner, K.J., Menviel, L., Morozova, P.A., Nisancioglu, K.H., O'Ishi, R., Mélia, D.S. Y., Shi, X., Sicard, M., Sime, L., Stepanek, C., Tomas, R., Volodin, E., Yeung, N.K.H., Zhang, Q., Zhang, Z., Zheng, W., 2021. Large-scale features of last Interglacial climate: results from evaluating the lig127k simulations for the coupled Model Intercomparison Project (CMIP6)-Paleoclimate Modeling Intercomparison Project (PMIP4). Clim. Past 17, 63–94. https://doi.org/10.5194/cp-17-63-2021.
Rayner, N.A., Parker, D.E., Horton, E.B., Folland, C.K., Alexander, L.V., Rowell, D.P., Kent, E.C., Kaplan, A., 2003. Global analyses of sea surface temperature, sea ice, and night marine air temperature since the late nineteenth century. J. Geophys. Res. Atmos. 108 https://doi.org/10.1029/2002jd002670.
Reimer, P.J., Bard, E., Bayliss, A., Beck, J.W., Blackwell, P.G., Ramsey, C.B., et al., 2013. IntCal13 and Marine13 radiocarbon age calibration curves 0–50,000 years cal BP. Radiocarbon 55 (04), 1869–1887. https://doi.org/10.2458/azu_js_rc.55.16947.
Rodrigues, R.R., Rothstein, L.M., Wimbush, M., 2007. Seasonal variability of the South Equatorial current bifurcation in the Atlantic Ocean: a numerical study. J. Phys. Oceanogr. 37 (1), 16–30. https://doi.org/10.1175/JPO2983.1.
Santos, T.P., Shimizu, M.H., Nascimento, R.A., Venancio, I.M., Campos, M.C., Portilho-Ramos, R.C., Ballalai, J.M., Lessa, D.O., Crivellari, S., Nagai, R.H., Chiessi, C.M., Kuhnert, H., Bahr, A., Albuquerque, A.L.S., 2022. A data-model perspective on the Brazilian margin surface warming from the Last Glacial Maximum to the Holocene. Quat. Sci. Rev. 285, 107557. https://doi.org/10.1016/j.quascirev.2022.107557.
Schlitzer, R., 2017. Ocean Data View. odv.awi.de.
Schneider, B., Leduc, G., Park, W., 2010. Disentangling seasonal signals in Holocene climate trends by satellite-model-proxy integration. Paleoceanography 25 (4). https://doi.org/10.1029/2009PA001893.
Stein, R., Fahl, K., Gierz, P., Niessen, F., Lohmann, G., 2017. Arctic Ocean sea ice cover during the penultimate glacial and the last interglacial. Nat. Commun. 8 (1), 1–13. https://doi.org/10.1038/s41467-017-00552-1.
Stramma, L., England, M., 1999. On the water masses and mean circulation of the South Atlantic Ocean. J. Geophys. Res. 104, 20.863–20.883. https://doi.org/10.1029/1999JC900139.
Sun, L., Alexander, M., Deser, C., 2018. Evolution of the global coupled climate response to Arctic Sea ice loss during 1990–2090 and its contribution to climate change. J. Clim. 31 (19), 7823–7843. https://doi.org/10.1175/JCLI-D-18-0134.1.
Tomas, R.A., Deser, C., Sun, L., 2016. The role of ocean heat transport in the global climate response to projected Arctic Sea ice loss. J. Clim. 29 (19), 6841–6859. https://doi.org/10.1175/JCLI-D-15-0651.1.
Turney, C.S.M., Jones, R.T., 2010. Does the Agulhas current amplify global temperatures during super-interglacials? J. Quat. Sci. 25, 839–843. https://doi.org/10.1002/jqs.1423.
Venancio, I.M., Belem, A.L., Santos, T.P., Lessa, D.O., Albuquerque, A.L.S., Mulitza, S., Schulz, M., Kucera, M., 2017. Calcification depths of planktonic foraminifera from the southwestern Atlantic derived from oxygen isotope analyses of sediment trap material. Mar. Micropaleontol. 136, 37–50. https://doi.org/10.1016/j.marmicro.2017.08.006.
Venancio, I.M., Mulitza, S., Govin, A., Santos, T.P., Lessa, D.O., Albuquerque, A.L.S., Chiessi, C.M., Tiedemann, R., Vahlenkamp, M., Bickert, T., Schulz, M., 2018. Millennial-to Orbital-Scale responses of Western Equatorial Atlantic Thermocline Depth to changes in the Trade Wind System since the last Interglacial. Paleoceanogr. Paleoclim. 33 (12), 1490–1507. https://doi.org/10.1029/2018PA003437.
Wang, K., Deser, C., Sun, L., Tomas, R.A., 2018. Fast response of the tropics to an abrupt loss of Arctic Sea ice via ocean dynamics. Geophys. Res. Lett. 45 (9), 4264–4272. https://doi.org/10.1029/2018GL077325.
Wolff, E.W., Fischer, H., Fundel, F., Ruth, U., Twarloh, B., Littot, G.C., Mulvaney, R., Röthlisberger, R., de Angelis, M., Boutron, C.F., Hansson, M., 2006. Southern Ocean sea-ice extent, productivity and iron flux over the past eight glacial cycles. Nature 440 (7083), 491–496. https://doi.org/10.1038/nature04614.
Žarić, S., Donner, B., Fischer, G., Mulitza, S., Wefer, G., 2005. Sensitivity of planktic foraminifera to sea surface temperature and export production as derived from sediment trap data. Mar. Micropaleontol. 55 (1–2), 75–105. https://doi.org/10.1016/j.marmicro.2005.01.002.
Zhang, D., Msadek, R., McPhaden, M.J., Delworth, T., 2011. Multidecadal variability of the North Brazil current and its connection to the Atlantic meridional overturning circulation. J. Geophys. Res. 116 (C4), 1–9. https://doi.org/10.1029/2010jc006812.
Zhang, X., Chen, F., 2021. Non-trivial role of internal climate feedback on interglacial temperature evolution. Nature 600 (7887), E1–E3. https://doi.org/10.1038/s41586-021-03930-4.